A Near-Field Meta-Steering Antenna System With Fully Metallic Metasurfaces

Foez Ahmed, *Graduate Student Member, IEEE*, Muhammad U. Afzal, *Senior Member, IEEE*, Touseef Hayat, *Graduate Student Member, IEEE*, Karu P. Esselle, *Fellow, IEEE*, and Dushmantha N. Thalakotuna, *Senior Member, IEEE*

***Abstract*— In the near-field meta-steering method, the near electric-field phase distribution is dynamically altered by rotating a pair of phase-gradient metasurfaces that are typically made out of dielectric lattices or metal patterns printed on bonded dielectric substrates. As a lightweight alternate, a new class of fully metallic metasurfaces (MMs) is proposed in this article. The lack of dielectrics not only substantially reduces the cost and weight but also increases its potential in space and high-power applications. More importantly, the new MMs are designed such that they can be made by cutting narrow slots in fully planar thin metal sheets, retaining structural rigidity while reducing the complexity, cost, and weight. The same MM works for any polarization. Each cell in the new MMs has close to ideal phase shift and transmission magnitude greater than −0.9 dB. A prototype was designed and fabricated to validate this MM-based beam-steering concept in the Ku-band. The maximum measured steering range in zenith is ±42°, with a full 360° steering in the azimuth. The measured 3 dB gain bandwidth is 700–800 MHz (5.6%–6.4%), and the measured gain variation (scan loss) when steering over the whole range is 2.2–4.5 dB. The weight density and thickness of each MM are 0.88 g/cm^2 and 0.8λ_0, respectively. Including the feed, the total antenna height is 4.9λ_0.**

***Index Terms*— Antenna, beam steering, dielectric-free metasurface, Ku-band, laser cut, lens, metallic manufacturing, metal-only, meta-steering system, phase correction surface (PCS), phase transformation, phase-shifting surface (PSS), polarization insensitive, satellite communication on-the-move (SOTM), wide angle.**

I. Introduction

BEAM-STEERING antennas have been a subject of extensive research due to their ability to provide uninterrupted data connectivity to moving platforms, including satellite communication on-the-move (SOTM) applications [1]–[3]. Beam-steering-enabled front-end antennas also ensure interference-free and secured end-to-end communication links. Traditional parabolic reflector dishes [4]–[6] commonly used in most applications need complicated tilting and rotation mechanisms and are bulky for moving platforms. Phased arrays [7]–[9] are preferred due to their planar low profile and ability to steer the beam quickly. Nevertheless, at higher microwave and millimeter-wave frequencies, phased arrays with high gains suffer from significant feed losses and are also expensive [10]. Reflect/transmit arrays (R/TAs) have several promising merits. However, in most cases, arrays are placed in the free space and illuminated by a horn antenna obeying a considerable focal distance, contributing to an increased overall height of the antenna system. Besides, in-plane translation and rotation of the feed and arrays to steer the beam in 2-D planes limit their deployment in volume constraint applications [11]–[16]. Recently, folded R/TAs have been investigated based on ray-folding design principles [17]–[19]. However, the beam was steered either by using active radio frequency (RF) components [17] or multiple feeding sources [18], [19] to resolve the feed/panel rotation and translation issues of conventional R/TAs.

In contrast to those classical approaches, a metasurface-based near-field phase transformation method, also known as near-field meta-steering (NFMS), has gained considerable interest since it was introduced in 2017 [20]. In these systems, two metasurfaces are placed very close to the aperture of a fixed-beam base antenna in its near-field region, leading to a planar, low-profile configuration. While the base antenna is fixed, the two metasurfaces are rotated independently to steer the antenna beam dynamically in the elevation and azimuth directions [20]–[26]. In most of the reported beam-steering antenna systems, the metasurface design strategy uses multiple dielectric and metal layers. In such designs, arrays of different metal patches, such as squares, are printed on dielectric slabs, and three or more such slabs are bonded together to form the metasurface. The need for low-loss dielectric slabs increases the system's overall cost and limits their use in some space and high-power microwave systems [27]–[29]. In addition, they need specialized manufacturing facilities to bond them into a single metasurface. The limited bandwidth of the original NFMS systems was successfully addressed using a pair of fully dielectric near-field phase transforming structures [24], [25]. However, the wedge-shaped stepped dielectric structures made antenna systems bulky and heavy and, hence, undermined some advantages of these antenna systems. A recently presented 30–40 GHz antenna system with two planar all-dielectric phase transformers addressed the

Manuscript received 19 November 2021; revised 9 May 2022; accepted 15 June 2022. Date of publication 29 June 2022; date of current version 17 November 2022. The work of Foez Ahmed was supported by the International Research Scholarship and Faculty of Engineering and Information Technology (FEIT) Scholarship. The work of Karu P. Esselle was supported by the Australian Research Council (ARC) Discovery Grant, Interactive High Performance Computing (iHPC) facility at UTS eResearch. *(Corresponding author: Foez Ahmed.)*

Foez Ahmed, Muhammad U. Afzal, Karu P. Esselle, and Dushmantha N. Thalakotuna are with the School of Electrical and Data Engineering, University of Technology Sydney, Sydney, NSW 2007, Australia (e-mail: foez.ahmed@student.uts.edu.au).

Touseef Hayat is with the School of Engineering, Macquarie University, Sydney, NSW 2109, Australia.

Color versions of one or more figures in this article are available at https://doi.org/10.1109/TAP.2022.3185502.

Digital Object Identifier 10.1109/TAP.2022.3185502

height limitation, but the weight of dielectric would still be significant if the antenna system is designed for high gain at 10–15 GHz frequencies [30].

An all-metal NFMS antenna system could be a potential candidate for low-cost, lightweight mobile systems as well as for high-power directive energy microwave systems. However, only one such has been successfully demonstrated so far [31], which was inspired by the original beam-steering system in [20]. This antenna has a pair of all-metal metasurfaces, each of which has four metal layers separated by 2-D arrays of waveguides. The presence of waveguides makes the metasurfaces nonplanar and heavy and, in addition, increases manufacturing complexity and overall cost. Moreover, in these all-metal metasurfaces, phase transformation is achieved by circularly polarized polarization conversion. Hence, each metasurface is limited to one sense of circular polarization for which it is designed (only RHCP or LHCP), and they cannot handle linear polarization at all. Phase transformation by polarization conversion is also known to have very limited bandwidth. Indeed, these are not limitations for the intended narrowband high-power applications in [31] but can limit their application to telecommunication systems.

This article aims to realize a high-performance 2-D beam-steering antenna system that can be fabricated at a low cost by designing mechanically robust, lightweight, and low-cost fully metallic metasurfaces (MMs). The novelty of this work is a new class of MMs that do not need any dielectric or expensive RF laminates as used in previously reported designs [20]–[22], hence cutting the cost of low-loss dielectric substrates significantly. Previous multilayered printed metasurfaces [20] made of RF laminates need specialized fabrication facilities to bond different layers into a single surface. The MMs reported in this article only need thin and cheap metal sheets. The novel slots-in-sheets (SiS)-type MMs have the required structural rigidity to self-support with only support needed at edges, where they do not impact the electromagnetic (EM) performance of the metasurface. It is an entirely different and new class of MM design strategy compared with other MMs reported in [31] that have used an array of bulky waveguides between two adjacent metal layers. The cells in the new MMs can provide a continuous and complete phase shift range from 0° to 360° with an excellent transmission magnitude larger than −1 dB, which is required in the NFMS system to mitigate adverse effects due to even small undesirable reflections from the metasurfaces. Furthermore, these MMs are used within the near-field region of the antenna, thus reducing the overall height of the antenna system compared to some other MMs that are used at least a few wavelengths away from the feed antenna. Unlike waveguide-type MMs [31] that are only compatible with circular polarization, the MMs proposed here can be used for circular and linear polarization, i.e., the steered beam direction is polarization independent. To the best of the authors' knowledge, fully 2-D MMs have never been investigated previously for NFMS antenna systems.

The demonstrated beam-steering antenna does not need active RF components or multiple feeding sources for beam steering. Measurements confirm that it can steer the beam in elevation to a maximum elevation angle of 42° and azimuth

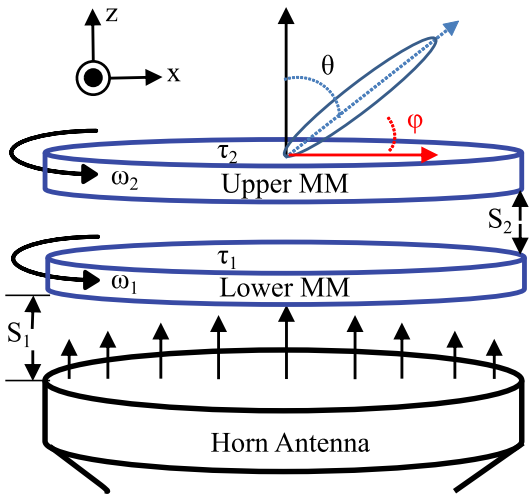

Fig. 1. Example for demonstrating the beam-steering principle using two independently rotatable MMs placed very close to the horn's aperture.

the whole 360°. The total electrical height of the proposed antenna system is only $4.9\lambda_0$, which is 41%, 66%, and 71% less than that of the recently reported beam-steering antenna systems in [24], [25], and [31], respectively.

The rest of this article is arranged as follows. Section II presents the configuration of the proposed beam-steering antenna system and explains the operating principle briefly. The design strategy of the metasurfaces and the impact of critical parameters are discussed in Section III. Section IV describes complete design examples, including the design of a customized 3-D printed conical horn antenna. Section V is on the fabrication of the prototype, and Section VI presents the measured results. Cross-polar rejection of the antenna system and the effect of metal conductivity on the system performance are studied in Section VII. Finally, this article is concluded in Section VIII.

II. Antenna Configuration

In order to evaluate the efficacy of the proposed MMs, a 2-D beam-steering antenna system is developed, which is inspired by the original near-field phase transformation method demonstrated in [20]. The configuration of the antenna system is shown in Fig. 1, which shows a pair of MMs placed very close to the aperture of a horn antenna with a fixed beam. S_1 represents the spacing between a base antenna and the first metasurface, and the spacing between the two metasurfaces is represented by S_2. The horn is static, while the pair of MMs are independently rotated around the z-axis to dynamically steer the beam to the desired azimuth and elevation angles within a large conical space.

The horn antenna creates an aperture field distribution, which is successively transformed by the two MMs. In principle, each MM introduces a linear phase progression to the near electric field, thus effectively tilting the beam to an offset angle. Since a typical horn suffers from a nonuniform phase profile in its aperture [32], the lower MM (LMM) has dual roles, i.e., phase correction in addition to the linear phase progression. The aperture phase distribution in a plane parallel

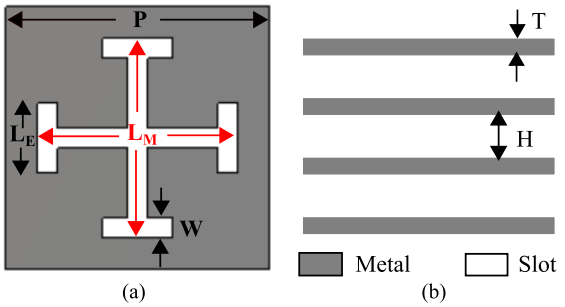

Fig. 2. Cell topology for a generic metallic phase-shifting cell: (a) top view and (b) side view showing four planar metallic layers separated by air gap of H.

to the antenna aperture is dynamically controlled by the relative angular positions (ω_1 and ω_2) of the two metasurfaces. A continuous rotation of one MM, keeping the other static, changes both elevation and azimuth angles of the beam. When both MMs are synchronously co-rotated by the same angle in the same direction, the beam azimuth angle changes between 0° and 360° without changing the elevation angle. Alternatively, when both MMs are synchronously counter-rotated with the same angle but in the opposite directions, the elevation angle of the beam is changed, while the azimuth angle remains the same [20], [33], [34].

III. Design of MMs

The key components of the NFMS antenna system are two new MMs made of metallic phase-shifting cells. The detailed design strategy and critical parametric studies of metallic cells and MMs are given in this section.

A. Metallic Phase-Shifting Cell

All phase-shifting cells in the metasurface have been designed with the aim to provide a continuous and complete 360° phase shift with an insertion loss of less than 1 dB. In addition, these cells do not require commercial dielectric laminates, and their mechanical robustness is ensured through the design strategy of introducing only narrow slots in thin and lightweight metal sheets.

The configuration of the metallic cell is shown in Fig. 2, which has a length (P) of $\lambda_0/2$ (=12 mm), where λ_0 is the free-space wavelength at the design frequency of 12.5 GHz. There are four identical thin planar sheets of metal, each having a thickness (T) of 0.3 mm ($=\lambda_0/80$) and separated by a distance (H) of 6 mm ($=\lambda_0/4$). It is to be mentioned here that the quarter-wavelength ($\lambda_0/4$) separation distance used between two metal layers in a metasurface is based on numerical simulations and analytical analysis reported in [35]. This is the optimal distance between adjacent layers of a quad-layer unit cell that can provide a complete 360° phase range with high transmission magnitude (>-1 dB) needed for the near-field metasurfaces. A Jerusalem-cross-shaped slot is etched in the middle of each metal sheet. The transmission through the cell was studied by analyzing it for unit-cell boundary conditions using full-wave simulations with the frequency-domain solver of CST Microwave Studio (MWS).

The number of minimum metal layers in the cell is critical to achieving the desired phase shift with the lowest insertion

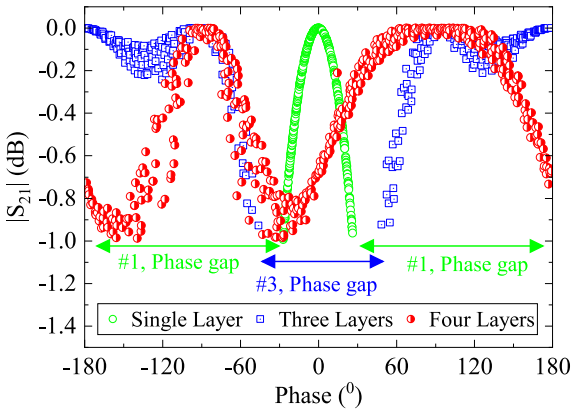

Fig. 3. Phase transmission coverage of the new metallic cells with a minimum transmission magnitude of -1 dB.

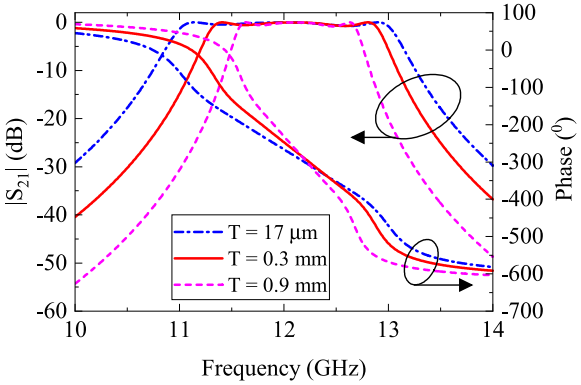

Fig. 4. Transmission magnitude and phase response for metal sheets with different thicknesses in a four-layer metallic cell.

loss. To understand the significance, we analyzed cells with one-, three-, and four identical metal layers in CST MWS. The width (W) of the slots in cells was fixed to 0.5 mm ($=\lambda_0/48$), and the lengths L_M and L_E were varied from 3 to 12 mm and from 1 to 9.5 mm, respectively. Some cells, where slots overlap within a cell or between adjacent cells, were not feasible and were excluded from the simulations. The phase of the transmission through cells is plotted against magnitude in Fig. 3. It is clear from the graph that cells with a single metal layer can provide phase shifts only in a limited range of around ±27°. Three-layer cells can continuously cover the phase range between ±46° and ±180° while maintaining a transmission magnitude greater than -1 dB, but they cannot cover a phase range of about 94° (see phase gap in Fig. 3). In contrast, four-layer cells cover the complete 360° phase range with high transmission magnitude.

Another critical parameter that impacts the transmission bandwidth and total phase range covered by the cell is the thickness of the metal sheets. To investigate this further, we simulated four-layer cells with three different metal thickness values. The transmission characteristics of these three cells are plotted in a frequency range around the operating frequency in Fig. 4. It is evident that cells with thinner metal sheets provide larger bandwidth and vice versa. It must, however, be mentioned that higher bandwidth comes at the cost of reduced mechanical stability and the need for additional support structures.

We considered cells with an intermediate thickness of 0.3 mm in the metasurfaces design presented in this article for

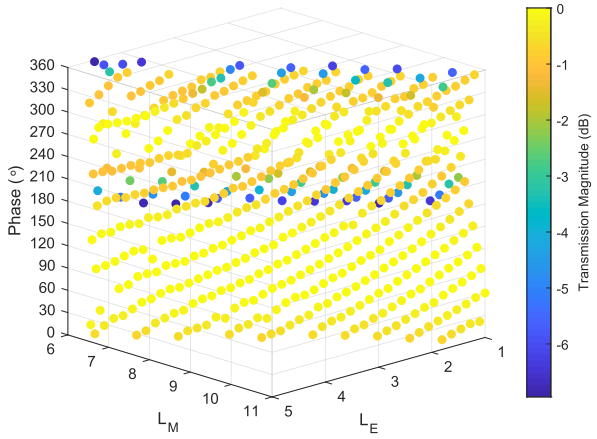

Fig. 5. Transmission magnitude and phase of metallic cells. The lengths of slots were swept as follows: $L_M = 6$–12 mm and $L_E = 1$–5 mm.

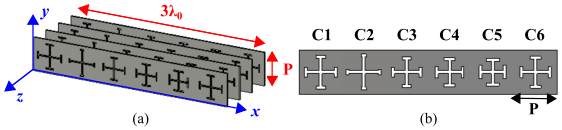

Fig. 6. Supercell topology: (a) stratified perspective view of four layers and (b) top view showing the corresponding unit-cell arrangement.

mechanical stability. At the design frequency of 12.5 GHz, the transmission magnitudes and phases of all viable cells against the two physical parameters are presented in Fig. 5. Each data point in the plot represents a cell with unique L_M and L_E. The data indicate that there exists a cell that provides any desirable phase value between 0° and 360° with a transmission magnitude > -1 dB (Fig. 5). Furthermore, the design approach ensures that the proposed cell topology is electrically invariant to a 90° rotation [36]; hence, it is polarization invariant, which is a highly desirable property for mobile systems.

B. Metallic Metasurfaces

A metasurface used for beam steering is a periodic 2-D array of identical supercells where each supercell is a 1-D array of n distinct cells. The number of individual cells (n) in a supercell can be determined by $n = 2\pi/\delta$ under the consideration of a complete cycle of 360° phase wrapping point in a metasurface. Here, δ denotes the phase difference between adjacent cells in a supercell that is defined by

$$\delta = dk_0 \sin(\tau) \tag{1}$$

where d denotes the interelement spacing, k_0 is the wavenumber in free space, and τ is the desired beam tilt angle of the metasurface.

For instance, due to the six discretized steps of phase shift, i.e., $\delta = 60°$, $n = 6$ cells are required to form a supercell to tilt the output beam to $\tau = 19.5°$ off-broadside direction. These six cells are selected from the prerecorded database (Fig. 5) in such a way that they have the highest transmission magnitude and a phase shift closest to the ideal phase shift. The first cell is assigned a phase of 15° to ensure that subsequent phases can be achieved with highly transmitting phase-shifting cells. Fig. 6 shows the supercell structure, and Table I gives the detailed parameters of each metallic cell at a design frequency of 12.5 GHz. All cells used in a supercell

TABLE I

DIMENSIONS AND TRANSMISSION COEFFICIENTS OF EACH CELL

Cells	Ideal Phase	Cell slot dimensions		Transmission coefficients	
		L_M	L_E	Actual Phase	$\lvert S_{21}\rvert$
	(°)	(mm)	(mm)	(°)	(dB)
C1	15	8.7	2.9	18	-0.391
C2	75	7.5	3.7	74	-0.001
C3	135	8.0	3.1	134	-0.091
C4	195	8.4	2.6	195	-0.901
C5	255	9.8	1.4	255	-0.057
C6	315	9.1	2.8	315	-0.578

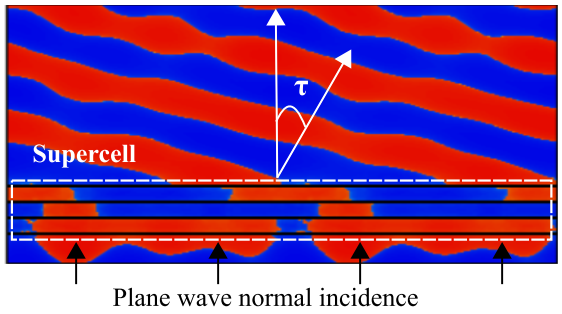

Fig. 7. Near electric-field (E_y) magnitude in a cross section of a supercell to verify 19.5° refraction at the design frequency of 12.5 GHz.

have a transmission magnitude greater than -0.9 dB, and the maximum difference between the ideal and actual phase is only 3°. The total length of the supercell is 72 mm ($=3\lambda_0$). It was simulated with CST MWS using the Floquet space harmonics and excited with fundamental TE mode propagating along the $+z$-axis to study its EM behavior.

The field propagation through the supercell is given in Fig. 7, which indicates that the outgoing field is tilted at an angle (τ) of 19.5°. The predicted far-field pattern through a finite-sized array of eight supercells along the x-axis is given in Fig. 8. The beam peak is at 19.5°, as expected. It is to be noted here that the far-field pattern in Fig. 8 is obtained by classical array theory, where patterns of a single supercell are multiplied with an array factor of 8 × 48 finite-sized arrays. To obtain this, we first simulate a supercell with periodic boundary conditions. The fields of the supercell are used to compute the far-field pattern of the element, which is then multiplied with an array factor of a finite-sized 8 × 48 rectangular array.

We have investigated the performance of six unit cells employed in MMs for TM and TE oblique incidence angles through full-wave EM simulations. The transmission coefficients of six unit cells are presented in Fig. 9 at the design frequency of 12.5 GHz for a maximum incident angle of 30°. The transmission coefficient magnitudes are almost constant and higher than -1 dB for TM incidence waves, as shown in Fig. 9(a). For TE incidence waves, the magnitude of transmission coefficient drops below -3 dB for the fifth unit cell for the incident angle larger than 15°. The maximum phase variation between the largest oblique and normal incidence angles of the TM waves is around 18°, as shown in Fig. 9(b). On the other hand, TE incidence waves are relatively more sensitive to oblique angles greater than 20°. The maximum phase variation remains about 18° for oblique angles less

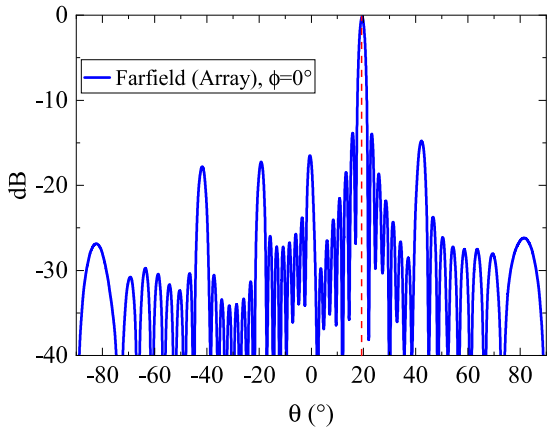

Fig. 8. Normalized far-field elevation pattern cut of a finite aperture at 12.5 GHz obtained from supercell simulations using array theory.

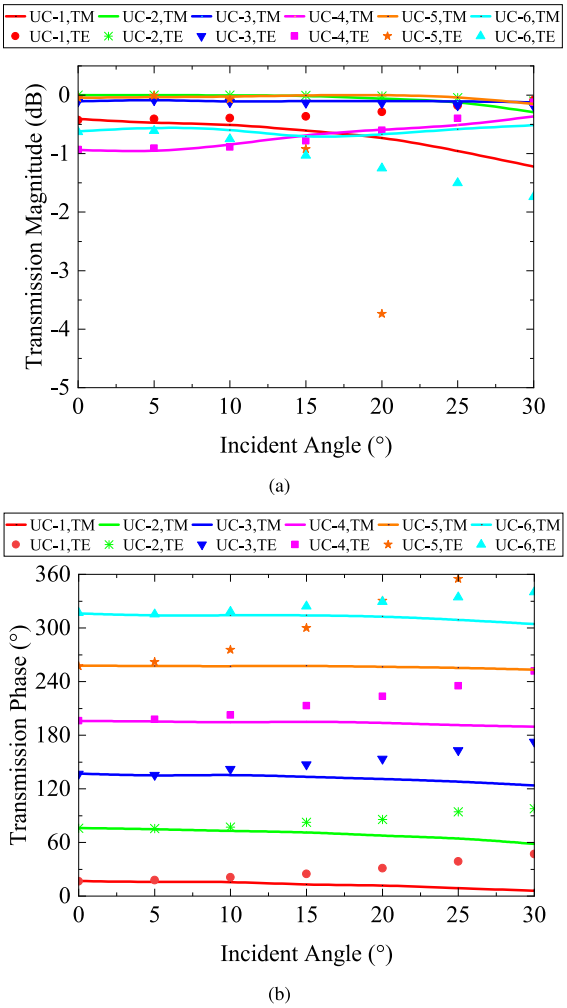

Fig. 9. Transmission (a) magnitude and (b) phase of six unit cells for oblique incidence at 12.5 GHz.

than 20° for all cells except fourth and fifth for the TE incidence waves. Compared with TM incidence waves, the phase response of the cells is more sensitive to larger oblique incidence angles of TE waves.

The supercell was arrayed to develop a metasurface for an aperture diameter of $6\lambda_0$ (=144 mm), which is the diameter of the horn discussed later in Section IV-A. The top view of the MM is shown in Fig. 10. For this aperture, two supercells are used along the x-axis and 12 along the y-axis. The MM is shaped to circular to match the aperture of the horn. Two identical metasurfaces can be used to steer the beam in an ideal base antenna with uniform aperture phase distribution. However, the horn does not have a uniform aperture phase distribution. Hence, this metasurface can only be used as the upper MM (UMM). In addition to providing linear phase progression, the lower metasurface must also correct the phase error in horn aperture field distribution, which is explained in Section IV. It is to be further noted here that cells of different dimensions are used in metasurface in contrast to the unit-cell simulation data where cells with periodic boundaries are simulated. This arrangement of different cells in the metasurface may create phase errors, which, based on our supercell simulations, are not significant in changing the beam direction.

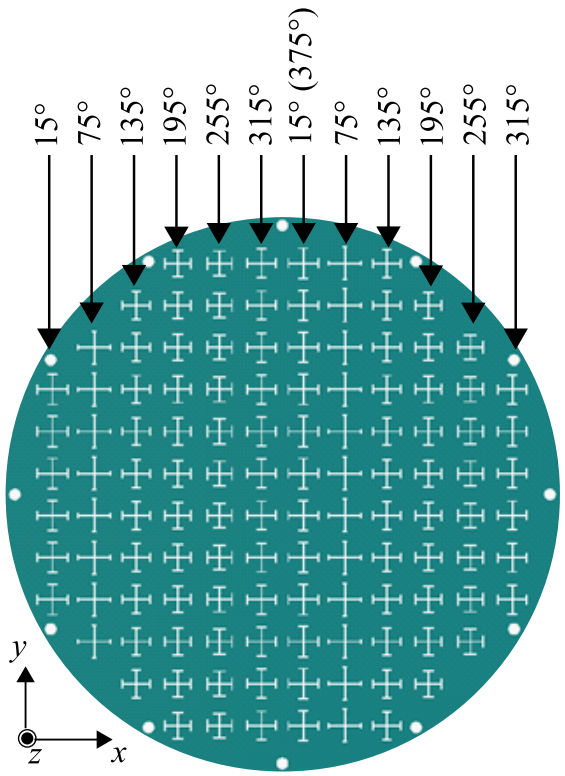

Fig. 10. Arrangement of supercells in the UMM to deflect the beam at an off-broadside direction of 19.5°.

IV. Design of the Antenna System

For concept demonstration, we have designed a conical horn antenna and fabricated it using low-cost equipment available in the laboratory. The design details of the horn and its compatible LMM are separately explained in Sections IV-A and IV-B.

A. Conical Horn

A conical horn with an aperture diameter (D) of 144 mm (=$6\lambda_0$) and the flare height (H) of 75 mm (=$3.125\lambda_0$) was designed to operate at 12.5 GHz. The horn was excited through a WR-75 waveguide-to-coaxial adapter, which is fixed to

r/c	1	2	3	4	5	6	7	8	9	10	11	12
1					350	350	350	350				
2			350	350	251	251	251	251	350	350		
3		350	251	251	168	168	168	168	251	251	350	
4		350	251	168	103	103	103	103	168	251	350	
5	350	251	168	103	103	57	57	103	103	168	251	350
6	350	251	168	103	57	37	37	57	103	168	251	350
7	350	251	168	103	57	37	37	57	103	168	251	350
8	350	251	168	103	103	57	57	103	103	168	251	350
9		350	251	168	103	103	103	103	168	251	350	
10		350	251	251	168	168	168	168	251	251	350	
11			350	350	251	251	251	251	350	350		
12					350	350	350	350				

Fig. 11. Phase distribution (12 × 12 cells) of a PCS that is required to correct the aperture phase nonuniformity of a horn.

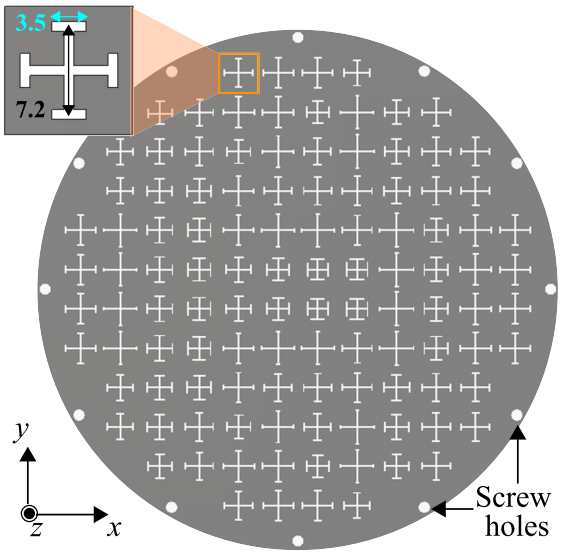

Fig. 12. Top view of the dual-mode LMM.

a 13.5 mm × 7.5 mm slot at the center of a metal sheet (Fig. 14). A 2 mm-thick circular base with a diameter of 50 mm was attached to the bottom part of the horn to screw the metal sheet and feed to the horn through four precut holes. The top of the horn cone has a 7.6 mm-wide extended circular edge with a thickness of 2.4 mm, which was created so that MMs can be securely attached to the horn in the near-field region. For this purpose, the edge ring has 12 holes separated by an angular spacing of 30°. A few design details and parameters are labeled in Fig. 14. The conical horn antenna was analyzed and optimized using the full-wave time-domain solver of CST MWS for the frequency range between 11.5 and 13.5 GHz.

B. Dual-Mode LMM

The LMM was designed for two simultaneous functions (phase correction and linear phase progression) following a three-step design process.

1) A linear phase progressive MM was designed following the design strategy explained in Section III-B. Its phase profile is indicated in Fig. 10. In this design example, τ is equal to 19.5°; hence, we can use the same phase difference δ to define a supercell discussed in Section III-B. Two supercells along the x-axis and 12 repetitions along the y-axis are required to cover the aperture of the horn.
2) A phase correction surface (PCS) was designed based on the nonuniform near-field aperture phase distribution of the horn, which was probed in a full-wave EM simulation. Its phase profile was recorded (Fig. 11). The design methodology for a PCS has been discussed at length in previous publications [37]–[39] and is not repeated here for brevity. The PCS diameter is kept the same as the horn aperture size. It is also noted that the four corner parts of PCS are truncated to make its shape circular, similar to the horn aperture.
3) The net phase profile $\Phi(r, c)$ of LMM was computed according to

$$\Phi(r, c) = \Phi_{MM}(r, c) + \Phi_{PCS}(r, c) \tag{2}$$

where $\Phi_{MM}(r, c)$ and $\Phi_{PCS}(r, c)$ denote the phase values of metallic cells in MM and PCS, respectively, at the (r, c) position in the 2-D coordinate system. For example, let us consider the first row and fifth column in Figs. 10 and 11. According to (2), the net phase shift required at this location is 605° (=255° + 350°), which is equivalent to a wrapped phase of 245°. A metallic cell with a 245° phase shift and the best possible transmission magnitude is found from the prerecorded database (i.e., the numerical equivalent of Fig. 5), and it is positioned at this location, as indicated in the inset of Fig. 12. The slot dimensions of this specific metallic cell are (L_M, L_E) = (7.2 mm, 3.5 mm). Likewise, all other metallic cells required for the LMM are found. It is worth emphasizing that we have only used phase-shifting cells with a transmission magnitude greater than −1 dB in all designs presented in this article. The top view of the LMM thus formed is shown in Fig. 12.

C. Impact of Interspacing Between Two Metasurfaces

For the configuration shown in Fig. 1, the spacings S_1 and S_2 impact the beam-steering performance on the system level. Theoretically, the parameter S_1 should not be changed as it is the distance where horn aperture phase distribution was probed as explained for the dual-mode LMM in Section IV-B. Hence, we fixed S_1 and increased S_2 from $\lambda/8$ to λ. We investigated the impact of S_2 for two extreme cases of beam steering when the beam peak is in the broadside ($\theta = 0°$) direction and steered to the $\theta = 38°$ direction. The pattern cuts for the two steering cases are plotted in Fig. 13. In the broadside case, the lowest S_2 has the highest gain/directivity with no significant change in the sidelobe levels (SLLs). On the contrary, peak gain/directivity improves with larger spacing when the beam is steered to 38° angles. We selected an intermediate value for the proposed system and fixed S_2 to $\lambda/6$ in the measured prototype. In an NFMS system, the aperture field distribution (amplitude and phase) influences the gain and direction of the beam peak. In this design approach, metasurfaces are formed ideally by selecting highly transmitting cells, where cells'

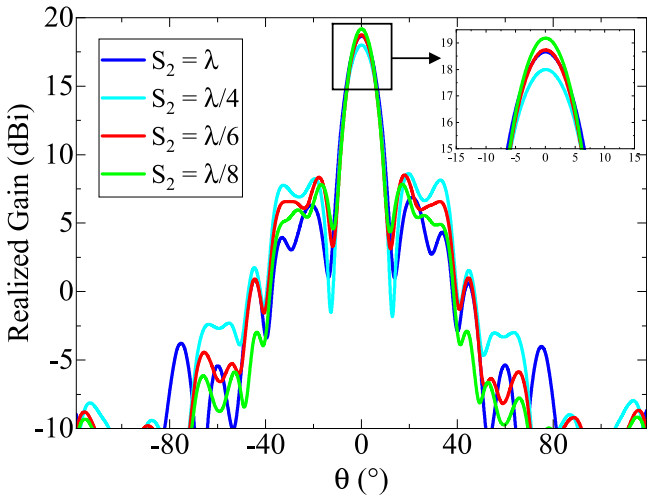

(a)

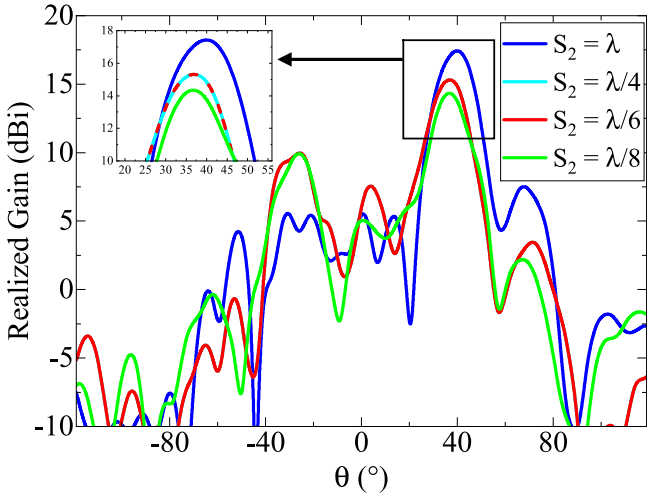

(b)

Fig. 13. Far-field pattern cuts of an antenna system for (a) broadside radiation and (b) 38° off-broadside radiation while interspacing between two MMs is varied from $\lambda/8$ to λ.

coupling effects between metasurfaces are ignored. This aspect impacts the phase and amplitude of the aperture field distribution in a practical system. The type of coupling is varied because the metasurfaces are physically rotated, which impacts the system gain differently. Therefore, the two cases demonstrated in Fig. 13 have different gain values for the same spacing between two metasurfaces. The extension of this research aims at using numerical optimization to address large gain variation even when metasurfaces are rotated to steer the beam.

V. Prototyping

The beam-steering performance of the antenna system was validated by fabricating and measuring the prototype shown in Fig. 14. The conical horn for the prototype was rapidly fabricated by 3-D printing using Omni3D [40] and polylactic acid (PLA) material. The PLA is an easily 3-D printable polymer, inexpensive, available locally, and widely used in various applications [41]. The plastic horn's inner surface was covered with thin layers of conductive copper tape. The overall weight of the horn is only 85.9 g. The performance of

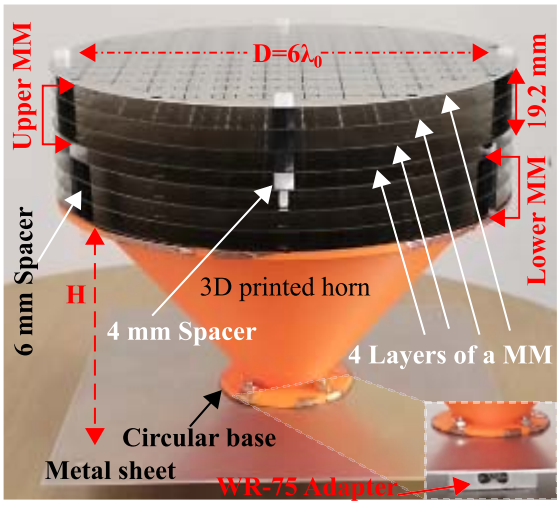

Fig. 14. Prototype of a 2-D beam-steering antenna system.

the horn without MMs was first verified by testing it in the antenna measurement chamber. These results are discussed in Section VI.

Eight layers (four in each MM are identical) needed for the two MMs were fabricated using high-precision laser cutting technology. These layers were developed by etching the narrow slots in an austenitic Grade 316 Stainless Steel (G316SS) sheet that has a thickness of 0.3 mm ($=\lambda_0/80$) $\pm 3\%$. The fabrication tolerance of the laser cutting machine is about ± 20 μm. For stacking sheets in each MM without any supporting structure in the middle part and for rotating MMs, 12 holes were created at the outer ring with an angular spacing of 30°. They are similar to and align with the holes on top of the horn antenna. Precise separations between adjacent layers of MMs were achieved using 6 mm ($=\lambda_0/4$) plastic spacers and screws inserted through the holes as mentioned above. The assembled MMs were then stacked on the horn with similar spacers and screws to complete prototyping. The LMM was placed very close to the horn, separated only by 1 mm ($S_1 = \lambda_0/24$) spacers. The UMM was placed 4 mm ($S_2 = \lambda_0/6$) away from the LMM. Each MM has a height of 19.2 mm ($=0.8\lambda_0$) and a weight of around 143.3 g, and including feed, the total antenna height is 118.4 mm ($\approx 4.9\lambda_0$). It is to be mentioned here that a large metal sheet at the bottom of the horn in Fig. 14 is not part of the EM design but included to firmly mount the prototype on the antenna under test (AUT) stage within the anechoic chamber.

VI. Measured Results

The antenna prototype was tested first by measuring its input impedance using a multiport vector network analyzer Agilent PNA-X N5242A. Then, pattern measurements were carried out in an MI far-field anechoic chamber at the Commonwealth Scientific and Industrial Research Organization (CSIRO).

First, the base horn antenna was measured. Its measured gain and VSWR are compared with predicted values obtained through full-wave simulations in Fig. 15. The measured results agree well with the predicted results.

The beam-steering performance was then validated in two steps. First, the antenna was measured only with the LMM

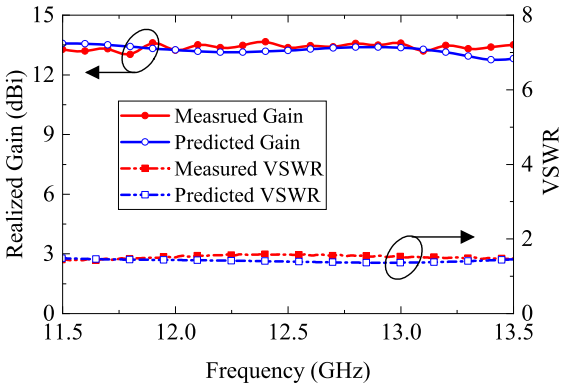

Fig. 15. Measured and predicted impedance matching and gain of horn antenna alone without MMs.

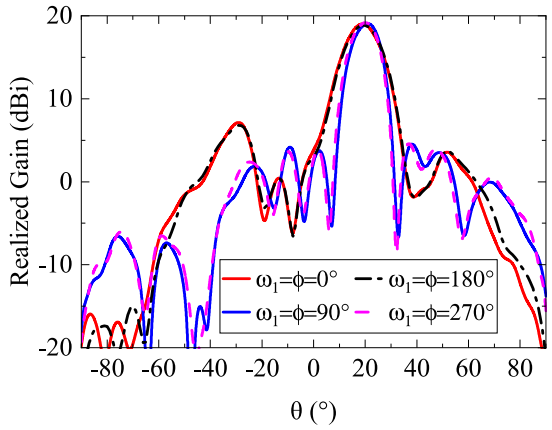

Fig. 16. Measured radiation pattern cuts in the elevation plane of the antenna system with only LMM at 12.5 GHz.

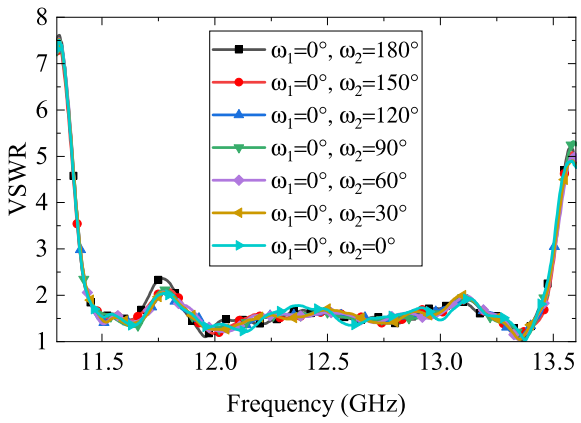

Fig. 17. Measured VSWR of the beam-steering antenna system. LMM is static ($\omega_1 = 0°$), and UMM is rotated from $\omega_2 = 0°$ to 180° in steps of 30°.

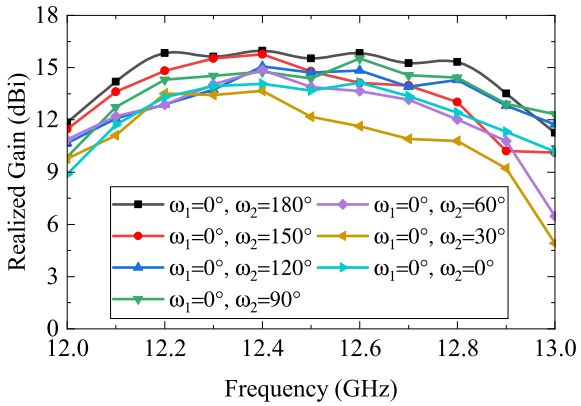

Fig. 18. Measured peak gain of the beam-steering antenna system. LMM is static ($\omega_1 = 0°$), and UMM is rotated from $\omega_2 = 0°$ to 180° in steps of 30°.

at the design frequency of 12.5 GHz. The elevation pattern cuts containing the beam peak are plotted in Fig. 16. These pattern cuts are taken for the different angular positions of the LMM at $\omega_1 = 0°$, 90°, 180°, and 270°. In all cases, the beam peak points at a 19.5° elevation angle, and the maximum variation in peak gain is less than 0.3 dBi. It is to be noted here that MM, even when placed within the near-field region of an antenna, deflects the antenna beam to an angle as predicted through generalized Snell's law [42]. The antenna exhibits its maximum peak gain of 19.18 dBi when the phase progression of the LMM aligns with the base antenna's E-plane (i.e., $\omega_1 = 90°$ and 270°). The SLL is at least 12.38 dB below the main beam.

The complete antenna system comprising the horn and two MMs was then measured to validate the 2-D beam-steering performance. The LMM was kept static above the horn (i.e., $\omega_1 = 0°$), and the UMM was rotated anticlockwise around the z-axis in 30° steps from $\omega_2 = 0°$ to 180°.

The VSWR shown in Fig. 17 was measured for seven angular positions of UMM, and it confirms that there is no significant effect on matching due to metasurface rotation. The measured input VSWR of the antenna is less than 2 from 11.44 to 13.46 GHz except for a small range of frequencies from 11.74 to 11.83 GHz. The clean 2:1 VSWR impedance matching bandwidth of the beam-steering antenna system is 13% (from 11.83 to 13.46 GHz), and it does not depend on rotation. It is worth mentioning that the coupling between the metasurfaces and horn antenna mainly affects the antenna input impedance matching, which is considered in predicting the overall antenna performance. The antenna input impedance is well-matched because of the very transparent nature of the proposed MMs. As a result, overall coupling effects due to metasurface loading are negligible, and hence, antenna performance is unaffected.

The radiation characteristics of the beam-steering antenna system were also tested over a wide frequency range. The measured realized peak gain is plotted in Fig. 18 over a frequency range between 12 and 13 GHz for seven different angular positions of UMM. The measured peak gain, 3 dB gain bandwidth, maximum peak gain, and the maximum gain variation of the prototype at each frequency within the band of interest are also summarized in Table II. The minimum and maximum 3 dB gain bandwidths are approximately 700 MHz (5.6%) and 800 MHz (6.4%), respectively at the center frequency of the operating band. The maximum measured peak gain of 16.0 dBi is noted, while the main beam is directed at $\theta = 0°$ (boresight) for $\omega_1 = 0°$ and $\omega_2 = 180°$. The gain changes a little when the beam is steered. The maximum gain variation measured at any frequency within the band is not more than 4.5 dBi. Table II also shows the maximum beam scanning ranges of the prototype at each frequency.

The radiation pattern cuts measured at elevation planes where beam peaks exist are plotted in Fig. 19 for nine

TABLE II
MEASURED PERFORMANCE OF THE BEAM-STEERING ANTENNA SYSTEM OVER A 900 MHZ FREQUENCY BAND

MMs Orientation	Frequency (GHz) vs. Peak Gain (dBi)									Max. Peak Gain	3-dB Gain BW	Fractional 3-dB Gain BW
	12.1	12.2	12.3	12.4	12.5	12.6	12.7	12.8	12.9	(dBi)	(MHz)	(%)
ω_1=0°, ω_2=180°	14.2	15.8	15.6	16.0	15.5	15.8	15.3	15.3	13.5	16.0	800	6.4
ω_1=0°, ω_2=150°	13.6	14.8	15.5	15.8	14.8	14.1	14.0	13.0	10.2	15.8	700	5.6
ω_1=0°, ω_2=120°	12.1	12.9	13.7	15.1	14.7	14.8	13.9	14.3	12.8	15.1	800	6.4
ω_1=0°, ω_2=90°	12.7	14.3	14.5	14.8	14.4	15.5	14.6	14.4	12.9	15.5	800	6.4
ω_1=0°, ω_2=60°	12.2	12.9	14.0	14.9	13.9	13.6	13.2	12.0	10.8	14.9	700	5.6
ω_1=0°, ω_2=30°	11.1	13.5	13.4	13.7	12.2	11.6	10.9	10.8	9.2	13.7	700	5.6
ω_1=0°, ω_2=0°	11.7	13.3	13.9	14.1	13.7	14.1	13.4	12.4	11.3	14.1	800	6.4
Max. Gain Variation (dBi)	3.1	3.0	2.2	2.3	3.3	4.2	4.3	4.5	4.3			
Beam Steering Range (°)	±41	±40	±42	±38	±39	±39	±41	±38	±42			

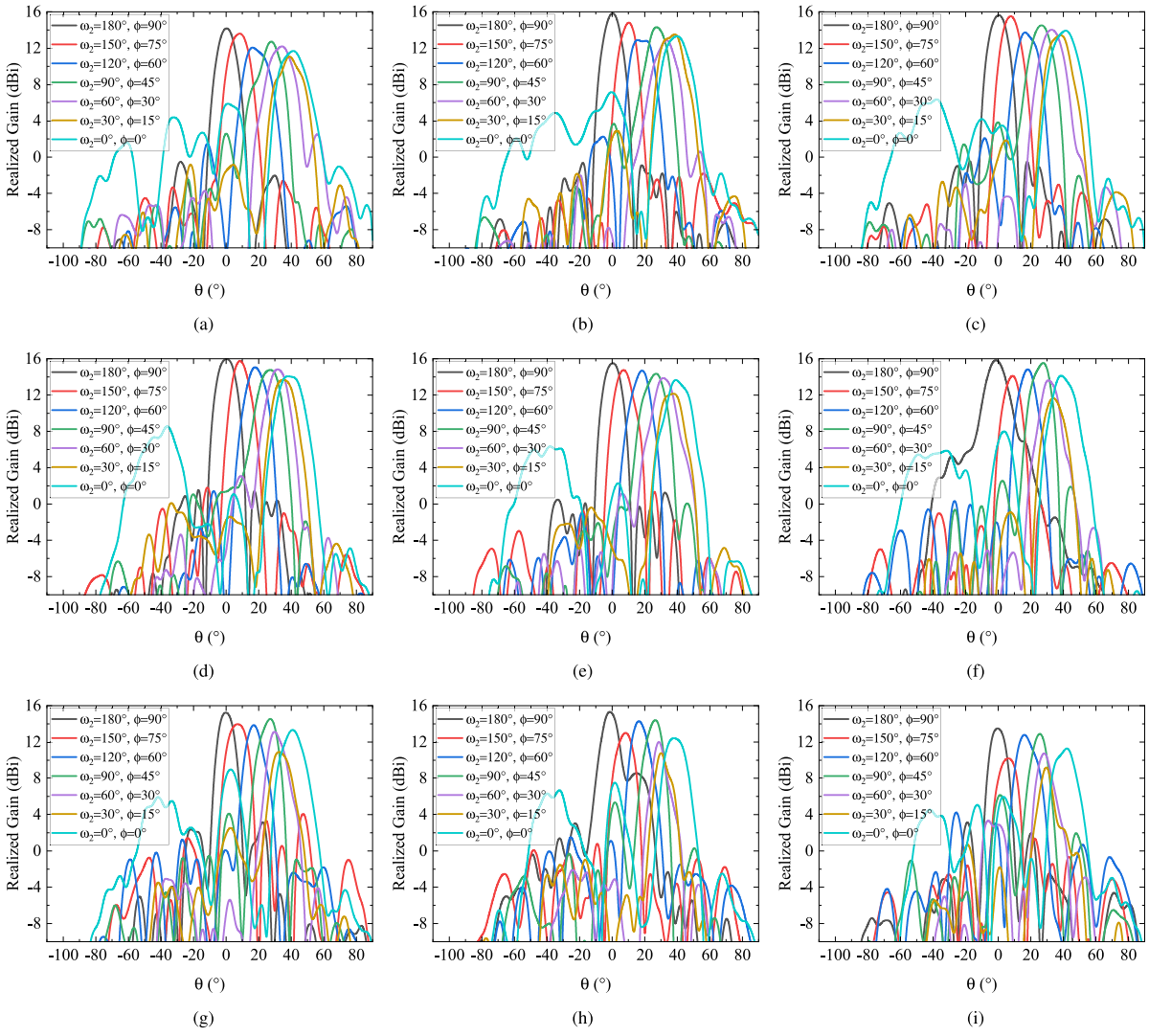

Fig. 19. Measured far-field pattern cuts of a beam-steering antenna while LMM is static at $\omega_1 = 0°$ and UMM is rotated from $\omega_2 = 0$ to 180° in steps of 30°. (a) 12.1 GHz. (b) 12.2 GHz. (c) 12.3 GHz. (d) 12.4 GHz. (e) 12.5 GHz. (f) 12.6 GHz. (g) 12.7 GHz. (h) 12.8 GHz. (i) 12.9 GHz.

frequencies between 12.1 and 12.9 GHz. The beam is highly directive, and SLLs are reasonably low for all frequencies except for the maximum tilt case of $\omega_2 = 0°$. This is common to many beam-steering systems based on metasurfaces. From Fig. 19, it is clear that the antenna can steer the beam within a large conical space ranging from 76° (±38°) to 84° (±42°), with very good pattern quality throughout the frequency band of interest. Overall, the experimental results have successfully validated the beam-steering concept with MMs.

The automated MMs rotation system is being separately developed in another project. The two MMs are attached to ring gears with a standard GT2 timing belt profile around

TABLE III
BEAM-STEERING ANTENNA SYSTEM PERFORMANCE COMPARISON WITH PUBLISHED WORKS

Ref.	Frequency (GHz)	Feed & Steering Method	MS/PT Types	MS/PT Thickness (λ_0) & Weight	Spacing Feed–MS1 (λ_0) & MS1–MS2 (λ_0)	Peak Gain (dBi)	Steering Range (El/Az) (^{0})	MS/PT Aperture Size (λ_0)	Aperture Efficiency (%)	Profile (λ_0)	Polarization
This work	**12.5**	**Horn NFMS-RP**	**All-Metal**	**0.8 light**	**0.04 0.17**	**18.8 (Sim) 16.0 (Mea)**	**±42/360**	**6.0**	**21.35 (Sim) 11.21 (Mea)**	**4.9**	**All LP/CP**
[31]	9.375	Horn TA-RP	All-Metal	0.94 heavy	0.63 1.25	–	±20/360	7.98	–	15.3	RHCP
[24]	30.0	WR28 NFMS-RP	Dielectric	1.07/1.17 bulky	1.0 –	16.0	±39/360	6.0	11.21	8.1	LP
[30]	34.5	Horn NFMS-RP	Dielectric	0.51 bulky	0.001 0.06	21.6	±54/360	5.9	42.0	10.2	All LP/CP
[14]	30.0	Patch Lens-TR	Composite	0.335 light	10.73 –	27.3	±50/360	19.5	–	8.4	RHCP
[20]	11.0	RCA NFMS-RP	Composite	0.12 heavy	0.29 0.15	19.4	±46/360	6.0	24.41	1.3	All LP/CP
[21]	12.5	CTSA NFMS-RP	Composite	0.214 heavy	0.17 –	17.8	±40/360	5.1	18.5	1.2	Dual LP
[22]	10.0	Horn Lens-RP	Composite	0.127 heavy	5.75 0.07	25.8	±60/360	11.5	29.1	6.1	All LP/CP

'–' data is not available, NFMS – Near-Field Meta-Steering, RP-Risley Prism, RCA – Resonant Cavity Antenna, CTSA – Continuous Transverse Stub Array TR-Translation and Rotation, MS/PT – Metasurface/Phase Transformer

the perimeter. The gears are then fixed to two lazy susan bearings. The base antenna is set on a base pad having an opening at the center for the RF cable, and the assembled MMs are placed on top at appropriate height using a stand placeholder. Two pancake stepper motors with suitable drivers are used to control the fine microstepping rotation of each MM through gears. For control signaling and communication among different modules, a microcontroller-based Arduino package is used.

VII. DISCUSSION

Table III shows a profile and performance comparison of the proposed beam-steering antenna system with previously published works. The predicted performance of the proposed system is comparable to most of the printed metasurface-based designs. The proposed system achieves this without using any dielectric that makes it suitable for intended low-cost and high-power applications. The antenna profile is also notably comparable with the beam-steering antenna systems using a similar type of feed.

The maximum height of the antenna is 118.4 mm ($\approx 4.9\lambda_0$), and its diameter (including extended edge for screws) is 159.2 mm. Even with auxiliary parts of the rotation system, the maximum height of the antenna does not change significantly. The height of the demonstrated antenna is approximately 84% less than the 750 mm tall commercially developed reflector-dish-based mechanically tilted and rotated antenna system [43]. The total weight of the proposed pair of MMs is around 286.6 g, which also allows the use of low-power compact motors, and hence, the overall weight of the antenna system will be much lighter than the weight of 100 kg system [43]. Moreover, unlike [14], [15], the antenna volume is always fixed during beam steering due to the lack of laterally moving parts.

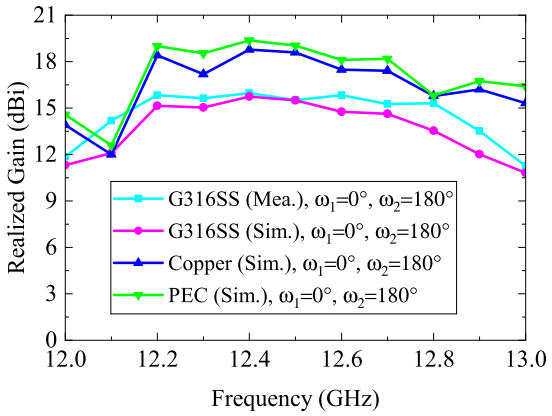

Fig. 20. Measured and predicted peak gain of antenna systems with different types of metallic materials. Beam peak is at $\theta = 0°$, while $\omega_1 = 0°$ and $\omega_2 = 180°$.

In all original simulations, the metal in the MMs was modeled as a perfect electric conductor (PEC). Those simulations, therefore, did not consider any losses in the MMs. The comparison of measured and predicted results for a PEC antenna indicates that there is approximately a 3.4 dB difference in measured and predicted maximum peak gain values. This issue was investigated later by modeling the actual MM material, G316SS, with a more accurate conductivity value. The agreement between measured and computed results was good, as shown in Figs. 20 and 21. The discrepancies can be attributed to the fabrication, assembling, and measurement tolerances.

Stainless Steel is an alloy typically used in metal manufacturing for its mechanical strength and resistance against rusting, and its conductivity is less than that of some other metals. The gain of this antenna beam-steering system can be increased significantly using a pure metal with higher conductivity, such as copper. To illustrate this, we simulated the

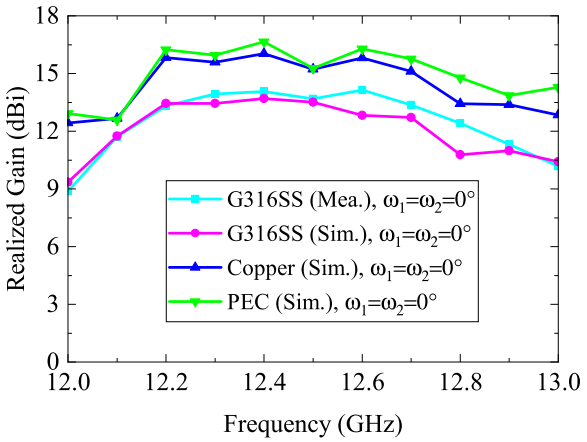

Fig. 21. Measured and predicted peak gain of antenna systems with different types of metallic materials. Beam peak is at $\theta = \pm 39°$, while $\omega_1 = 0°$ and $\omega_2 = 0°$.

TABLE IV
MATERIAL PROPERTIES OF COPPER AND G316SS

Property	Copper	G316SS
Electric Conductivity (S/m)	5.8×10^7	1.32×10^6
Material Density (kg/m^3)	8930	8070
Thermal Conductivity (W/K/m)	401	17
Heat Capacity (kJ/K/kg)	0.39	0.53
Thermal Diffusivity (m^2/s)	1.1514×10^{-4}	3.97466×10^{-6}
Young's Modulus (kN/mm^2)	120	193

same antenna system with three different conductive materials for the MMs: PEC, copper, and Stainless Steel G316SS. The detailed thermophysical properties of these materials are listed in Table IV [44]–[46].

Two extreme beam-steering cases, i.e., when the beam is at the broadside ($\theta = 0°$) direction and the beam is at the farthest from the broadside direction ($\theta = \pm 39°$), were simulated with each material. The predicted results of the beam-steering antenna systems using new material models for the metal metasurfaces are also shown in Figs. 20 and 21 for the two extreme cases.

From Fig. 20, it is further apparent that the maximum peak gain expected from copper MMs in the boresight direction is 18.8 dBi, which is significantly greater than the maximum peak gain of 16 dBi achievable using G316SS. A significant improvement is also noted in Fig. 21 for the maximum beam tilt situation if copper replaces G316SS. Furthermore, this study indicates that the copper MMs produce performance very close to the ideal PEC MMs. The reason for the lower gain of the prototype is that the conductivity of G316SS is 1/44th of the conductivity of copper.

The predicted and measured pattern cuts of the antenna system taken at the design frequency of 12.5 GHz are compared in Fig. 22. The measured pattern cuts are in excellent agreement with the predicted results. The maximum measured SLL is -7.9 dB when the beam is tilted to the maximum elevation angle. In all other cases, SLL is at least 12.6 dB below the main beam. A comparison of measured and predicted beam directions is given in Table V. The maximum difference in

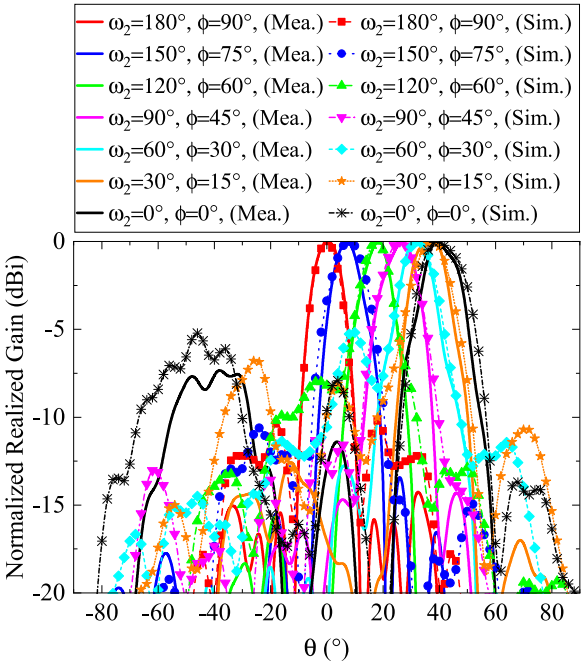

Fig. 22. Measured and predicted normalized radiation pattern cuts at 12.5 GHz for seven angular positions of UMM, while LMM is static ($\omega_1 = 0°$). MMs are modeled and fabricated using G316SS.

TABLE V
BEAM POSITION COMPARISON AT 12.5 GHZ. LMM IS STATIC AT $\omega_1 = 0°$, AND UMM IS ROTATED FROM $\omega_2 = 0$ TO 180°

Orientation of MMs		Predicted		Measured	
ω_1 (°)	ω_2 (°)	θ (°)	ϕ (°)	θ (°)	ϕ (°)
0	0	39	0	39	0
0	30	38	15	38	15
0	60	32	30	31	30
0	90	26	45	27	45
0	120	18	60	18	60
0	150	8	75	7	75
0	180	0	90	0	90

TABLE VI
CROSS-POLAR DISCRIMINATION AT 12.5 GHZ. LMM IS STATIC AT $\omega_1 = 0°$, AND UMM IS ROTATED FROM $\omega_2 = 0°$ TO 180°

Main Beam Direction (°)	Co-polar Gain (dBi)	Cross-polar Gain (dBi)	Cross-polar Discrimination (dB)
0	15.5	-37.0	52.5
18	14.5	-1.8	16.3
31	12.8	-2.4	15.2
39	13.5	-30.0	43.5

the direction of the beam peaks in predicted and measured results is not more than 1°. Overall, the predicted and measured results successfully validate the concept of the proposed beam-steering using fully MMs.

In order to understand how this method of beam steering affects antenna polarization, we have tracked the cross-polar level as we steer the beam of this linearly polarized antenna

away from the broadside direction. The results are summarized in Table VI. It can be seen that although cross-polar level changes with beam steering, the antenna maintains good cross-polar discrimination in all beam directions.

VIII. Conclusion

This article presents a class of planar fully MMs that can be positioned in the near-field region of an antenna, very close to its aperture, to design a high-performance beam-steering antenna system. The proof-of-concept antenna system is made of a horn antenna and a pair of MMs that are placed at $\lambda_0/24$ spacing from the horn antenna. The design consideration of the metasurfaces is such that they do not need any mechanical supporting structures or dielectric substrates even if the aperture size is considerably large. The required mechanical robustness was achieved by designing a new class of MMs composed of narrow slots cut in metal sheets. The use of four identical metal layers in each metasurface also reduces the complexity, prototyping cost, and large-scale production cost. The demonstrated system is a significant step toward a low-cost, lightweight, NFMS system and a radical departure from traditional dielectric-based metasurfaces commonly used in such systems. The measured results indicate that the proposed system has good overall bandwidth and can steer the beam in a large apex angle ranging from 76° to 84° while maintaining acceptable pattern quality within the operating band of interest. Although the measured maximum peak gain of the system is 16 dBi, it can be significantly increased using a large aperture base antenna (instead of the horn used here) or an array and a pure metal with higher conductivity, such as copper.

Acknowledgment

The authors would like to thank Ken Smart from the Commonwealth Scientific and Industrial Research Organization (CSIRO) for valuable discussion and prototype measurements support.

References

[1] D. G. Lockie, M. Sereno, and M. Thomson, "Spacecraft antennas and beam steering methods for satellite communication system," U.S. Patent 5 642 122, Jun. 24, 1997.

[2] D. C. Law *et al.*, "An electronically stabilized phased array system for shipborne atmospheric wind profiling," *J. Atmos. Ocean. Technol.*, vol. 19, pp. 924–933, Jun. 2002.

[3] X. Flores-vidal, P. Flament, R. Durazo, C. Chavanne, and K. W. Gurgel, "High-frequency radars: Beamforming calibrations using ships as reflectors," *J. Atmos. Ocean. Technol.*, vol. 30, no. 3, pp. 638–648, Mar. 2013.

[4] A. W. Rudge and M. J. Withers, "New technique for beam steering with fixed parabolic reflectors," *Proc. Inst. Electr. Eng.*, vol. 118, no. 7, pp. 857–863, Jul. 1971.

[5] W. L. Pritchard, "Satellite communication—An overview of the problems and programs," *Proc. IEEE*, vol. 65, no. 3, pp. 294–307, Mar. 1977.

[6] J. Duggan and P. McLane, "Adaptive beamforming with a multiple beam antenna," in *Proc. Int. Conf. Commun.*, vol. 1, 1998, pp. 395–401.

[7] A. I. Zaghloul, O. Kilic, and E. C. Kohls, "System aspects and transmission impairments of active phased arrays for satellite communications," *IEEE Trans. Aerosp. Electron. Syst.*, vol. 43, no. 1, pp. 176–186, Jan. 2007.

[8] R. C. Hansen, *Phased Array Antennas*, 2nd ed. Hoboken, NJ, USA: Wiley, Nov. 2009.

[9] E. Topak, J. Hasch, C. Wagner, and T. Zwick, "A novel millimeter-wave dual-fed phased array for beam steering," *IEEE Trans. Microw. Theory Techn.*, vol. 61, no. 8, pp. 3140–3147, Aug. 2013.

[10] C. Henry. (2017). *Panasonic Avionics: 'Jury's Still Out' on Profitability of in-Flight Connectivity*. [Online]. Available: https://spacenews.com/panasonic-avionics-jurys-still-out-on-profitability-of-in-flight-connectivity/

[11] X. Yang *et al.*, "A mechanically reconfigurable reflectarray with slotted patches of tunable height," *IEEE Antennas Wireless Propag. Lett.*, vol. 17, no. 4, pp. 555–558, Apr. 2018.

[12] P. Mei, S. Zhang, and G. F. Pedersen, "A low-cost, high-efficiency and full-metal reflectarray antenna with mechanically 2-D beam-steerable capabilities for 5G applications," *IEEE Trans. Antennas Propag.*, vol. 68, no. 10, pp. 6997–7006, Oct. 2020.

[13] M. E. Trampler, R. E. Lovato, and X. Gong, "Dual-resonance continuously beam-scanning X-band reflectarray antenna," *IEEE Trans. Antennas Propag.*, vol. 68, no. 8, pp. 6080–6087, Aug. 2020.

[14] E. B. Lima, S. A. Matos, J. R. Costa, C. A. Fernandes, and N. J. G. Fonseca, "Circular polarization wide-angle beam steering at Ka-band by in-plane translation of a plate lens antenna," *IEEE Trans. Antennas Propag.*, vol. 63, no. 12, pp. 5443–5455, Dec. 2015.

[15] S. A. Matos *et al.*, "High gain dual-band beam-steering transmit array for satcom terminals at Ka-band," *IEEE Trans. Antennas Propag.*, vol. 65, no. 7, pp. 3528–3539, Jul. 2017.

[16] P. Naseri, S. A. Matos, J. R. Costa, and C. A. Fernandes, "Phase-delay versus phase-rotation cells for circular polarization transmit arrays—Application to satellite Ka-band beam steering," *IEEE Trans. Antennas Propag.*, vol. 66, no. 3, pp. 1236–1247, Mar. 2018.

[17] Z. Wang *et al.*, "1 bit electronically reconfigurable folded reflectarray antenna based on p-i-n diodes for wide-angle beam-scanning applications," *IEEE Trans. Antennas Propag.*, vol. 68, no. 9, pp. 6806–6810, Sep. 2020.

[18] P. Mei, S. Zhang, and G. F. Pedersen, "A low-profile and beam-steerable transmitarray antenna: Design, fabrication, and measurement [antenna applications corner]," *IEEE Antennas Propag. Mag.*, vol. 63, no. 5, pp. 88–101, Oct. 2021.

[19] G. Li, Y. Ge, and Z. Chen, "A compact multibeam folded transmitarray antenna at Ku-band," *IEEE Antennas Wireless Propag. Lett.*, vol. 20, no. 5, pp. 808–812, May 2021.

[20] M. U. Afzal and K. P. Esselle, "Steering the beam of medium-to-high gain antennas using near-field phase transformation," *IEEE Trans. Antennas. Propag.*, vol. 65, no. 4, pp. 1680–1690, Apr. 2017.

[21] T. Lou, X.-X. Yang, H. Qiu, Z. Yin, and S. Gao, "Compact dual-polarized continuous transverse stub array with 2-D beam scanning," *IEEE Trans. Antennas Propag.*, vol. 67, no. 5, pp. 3000–3010, May 2019.

[22] Z. Zhang, H. Luyen, J. H. Booske, and N. Behdad, "X-band, mechanically-beam-steerable lens antenna exploiting the Risley prism concept," *IET Microw., Antennas Propag.*, vol. 14, no. 14, pp. 1902–1908, Oct. 2020.

[23] M. U. Afzal, A. Lalbakhsh, and K. P. Esselle, "Electromagnetic-wave beam-scanning antenna using near-field rotatable graded-dielectric plates," *J. Appl. Phys.*, vol. 124, no. 23, pp. 234901–234911, Dec. 2018.

[24] M. U. Afzal, L. Matekovits, K. P. Esselle, and A. Lalbakhsh, "Beam-scanning antenna based on near-electric field phase transformation and refraction of electromagnetic wave through dielectric structures," *IEEE Access*, vol. 8, pp. 199242–199253, 2020.

[25] A. A. Baba, R. M. Hashmi, K. P. Esselle, M. Attygalle, and D. Borg, "A millimeter-wave antenna system for wideband 2-D beam steering," *IEEE Trans. Antennas Propag.*, vol. 68, no. 5, pp. 3453–3464, May 2020.

[26] M. Akbari, M. Farahani, A. Ghayekhloo, S. Zarbakhsh, A. R. Sebak, and T. A. Denidni, "Beam tilting approaches based on phase gradient surface for mmWave antennas," *IEEE Trans. Antennas Propag.*, vol. 68, no. 6, pp. 4372–4385, Jun. 2020.

[27] S. Levine, "The active denial system a revolutionary, non-lethal weapon for today's battlefield," Center Technol. Nat. Secur. Policy, Nat. Defense Univ., Washington, DC, USA, Tech. Rep. ADA501865 and OMB 0704-0188, Jun. 2009. [Online]. Available: http://www.dtic.mil/docs/citations/ADA501865

[28] N. Chamberlain, J. Chen, R. Hodges, R. Hughes, and J. Jakoboski, "Juno microwave radiometer all-metal patch array antennas," in *Proc. IEEE Antennas Propag. Soc. Int. Symp.*, Jan. 2008, pp. 1–4.

[29] N. Chahat, B. Cook, H. Lim, and P. Estabrook, "All-metal dual-frequency RHCP high-gain antenna for a potential Europa Lander," *IEEE Trans. Antennas Propag.*, vol. 66, no. 12, pp. 6791–6798, Dec. 2018.

[30] A. A. Baba, R. M. Hashmi, M. Attygalle, K. P. Esselle, and D. Borg, "Ultrawideband beam steering at mm-wave frequency with planar dielectric phase transformers," *IEEE Trans. Antennas Propag.*, vol. 70, no. 3, pp. 1719–1728, Mar. 2022.

[31] X. Zhao *et al.*, "All-metal beam steering lens antenna for high power microwave applications," *IEEE Trans. Antennas Propag.*, vol. 65, no. 12, pp. 7340–7344, Dec. 2017.
[32] K. Liu, Y. Ge, and C. Lin, "A compact wideband high-gain metasurface-lens-corrected conical horn antenna," *IEEE Antennas Wireless Propag. Lett.*, vol. 18, no. 3, pp. 457–461, Mar. 2019.
[33] N. Gagnon and A. Petosa, "Using rotatable planar phase shifting surfaces to steer a high-gain beam," *IEEE Trans. Antennas Propag.*, vol. 61, no. 6, pp. 3086–3092, Jun. 2013.
[34] J. Wang and Y. Ramhat-Samii, "Phase method: A more precise beam steering model for phase-delay metasurface based Risley antenna," in *Proc. URSI Int. Symp. Electromagn. Theory*, May 2019, pp. 1–4.
[35] A. H. Abdelrahman, A. Z. Elsherbeni, and F. Yang, "Transmission phase limit of multilayer frequency-selective surfaces for transmitarray designs," *IEEE Trans. Antennas Propag.*, vol. 62, no. 2, pp. 690–697, Feb. 2014.
[36] J. Perruisseau-Carrier, "Optimal cell topology constraint for monolayer dual-polarized beamscanning reflectarrays," *IEEE Antennas Wireless Propag. Lett.*, vol. 11, pp. 434–437, 2012.
[37] M. U. Afzal, K. P. Esselle, and B. A. Zeb, "Dielectric phase-correcting structures for electromagnetic band gap resonator antennas," *IEEE Trans. Antennas Propag.*, vol. 63, no. 8, pp. 3390–3399, Aug. 2015.
[38] M. U. Afzal and K. P. Esselle, "A low-profile printed planar phase correcting surface to improve directive radiation characteristics of electromagnetic band gap resonator antennas," *IEEE Trans. Antennas Propag.*, vol. 64, no. 1, pp. 276–280, Jan. 2016.
[39] F. Ahmed, M. U. Afzal, T. Hayat, K. P. Esselle, and D. N. Thalakotuna, "A dielectric free near field phase transforming structure for wideband gain enhancement of antennas," *Sci. Rep.*, vol. 11, no. 1, pp. 1–13, Jul. 2021.
[40] Omni3D. *Omni3D-Large Industrial 3D Printers*. Accessed: Jun. 28, 2022. [Online]. Available: https://omni3d.com/
[41] M. Mirzaee and S. Noghanian, "High frequency characterisation of wood-fill PLA for antenna additive manufacturing application," *Electron. Lett.*, vol. 52, no. 20, pp. 1656–1658, Sep. 2016.
[42] N. Yu *et al.*, "Light propagation with phase discontinuities: Generalized laws of reflection and refraction," *Science*, vol. 334, no. 6054, pp. 333–337, Oct. 2011.
[43] *Satcom-on-the-Move: A Terminal Engineered to Sing*, EMSolution, San Jose, CA, USA, Aug. 2012.
[44] C. S. Kim, "Thermophysical properties of stainless steels," Argonne Nat. Lab., U.S. Energy Res. Develop. Admin., Lemont, IL, USA, Tech. Rep. ANL-75-55, Sep. 1975.
[45] K. M. Ralls, T. H. Courtney, and J. Wulff, *An Introduction to Materials Science and Engineering*. New York, NY, USA: Wiley, 1976.
[46] W. D. Callister, *Materials Science and Engineering: An Introduction*, 10th ed. New York, NY, USA: Wiley, Jan. 2018.

Foez Ahmed (Graduate Student Member, IEEE) received the B.Sc. (Hons.) and M.Sc. degrees in information and communication engineering from the University of Rajshahi (RU), Rajshahi, Bangladesh, in 2007 and 2009, respectively, and the M.Eng. degree in electrical and computer engineering from the South China University of Technology (SCUT), Guangzhou, China, in 2013. He is currently pursuing the Ph.D. degree with the School of Electrical and Data Engineering, University of Technology Sydney (UTS), Sydney, NSW, Australia.

From 2012 to 2014, he was a Lecturer with the Department of Information and Communication Engineering, RU, where he has been an Assistant Professor since 2014 (now on study leave). He was also a Lecturer at the Northern University of Bangladesh, Dhaka, Bangladesh, from 2008 to 2009, and King Khalid University, Abha, Saudi Arabia, from 2009 to 2011. His current research interests include high-gain antennas, SATCOM antennas, metasurfaces, frequency-selective surfaces, and far-field pattern synthesis using near-field phase transformation.

Mr. Ahmed was a recipient of several prestigious awards and scholarships, including the Commonwealth-funded International Research Training Program (iRTP) Scholarship; the International Research Scholarship (IRS) and the Faculty of Engineering and Information Technology (FEIT) Scholarship from the University of Technology Sydney; the Gold Medal from the University of Rajshahi, the Chinese Government Scholarship; the Academic Achievement Award, and the Excellency Award from SCUT, China.

Muhammad U. Afzal (Senior Member, IEEE) received the bachelor's degree (Hons.) in electronics engineering and the master's degree in computational science and engineering from the National University of Sciences and Technology (NUST), Islamabad, Pakistan, in 2009 and 2011, respectively, and the Ph.D. degree in electronics engineering from Macquarie University, Sydney, NSW, Australia, in 2017.

He is currently a Research Fellow working at the University of Technology Sydney, Sydney. He developed the concept of near-field phase transformation during his doctorate research, which was demonstrated to enhance the directivity of low-gain aperture antennas in IEEE TRANSACTIONS ON ANTENNAS AND PROPAGATION paper entitled "Dielectric phase-correcting structures for electromagnetic band-gap resonator antennas." To commercialize the outcomes of his research, he led a team of colleagues in a CSIRO sponsored ON Prime 2 in 2017—a preaccelerator program designed to commercialize outcomes of academic research in Australia. He started his professional career as a Lab Engineer at the Research Institute for Microwave and Millimetre-Wave Studies (RIMMS), NUST, in 2010. In 2012, he was promoted to the position of Lecturer, which he continued until February 2013. In 2017, after his Ph.D. degree, he was offered a post-doctorate for three years on a project funded by the Australian Research Council (ARC) through the Discovery Grant Scheme at Macquarie University. Apart from the project-specific research, he co-supervised one Ph.D., three masters of research, and several undergraduate thesis students at Macquarie University. He was the third CI in a team of five who received a grant of more than $20k from the German Academic Exchange Service in a funding scheme "Australia-Germany Joint Research Co-Operation Scheme." He is the co-inventor of efficient antenna beam-steering technology referred to as near-field meta-steering. This technology received the "Highly Commended" certificate in the Five Future-Shaping Research Priorities category in the 2017 Academic Staff Awards at Macquarie University. He is currently working on the development of satellite-terminal antenna technology and has research interests in electromagnetic phase-shifting structures, frequency-selective surfaces, and similar metamaterials for microwave and millimeter-wave antenna applications.

Dr. Afzal has received several awards and scholarships, including a merit-based scholarship in six out of eight semesters during the undergraduate degree, a scholarship of complete fee waiver during the postgraduate degree, and the International Macquarie Research Excellence (iMQRES) Scholarship toward the doctorate study from Macquarie University. He received a Competitive Travel Grant in 2015 to present my research work at a flagship conference under the Antennas and Propagation Society (APS) in Vancouver, BC, Canada. He assisted in preparing several grant applications, including a successful ARC Discovery Grant in 2018.

Touseef Hayat (Graduate Student Member, IEEE) received the B.S. degree in telecommunication engineering from the University of Engineering and Technology, Taxila, Pakistan, in 2014, the M.S. degree (Hons.) from the National University of Sciences and Technology (NUST), Islamabad, Pakistan, in 2016, and the Master of Research (M.Res.) degree (Hons.) in electronics engineering from Macquarie University, Sydney, NSW, Australia, in 2018, where he is currently pursuing the Ph.D. degree.

His research interests include electromagnetic-bandgap resonant antennas, additive manufacturing of microwave components, phase and amplitude transforming metasurfaces, and dielectric characterization.

Mr. Hayat received several prestigious awards, including the International Research Training Program Scholarship (iRTP) for his M.Res. degree and the International Macquarie University Research Excellence Scholarship (iMQRES) for his Ph.D. degree.

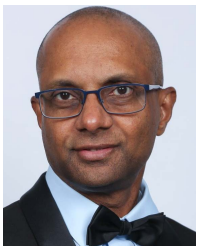

Karu P. Esselle (Fellow, IEEE) received the B.Sc. degree (Hons.) in electronic and telecommunication engineering from the University of Moratuwa, Moratuwa, Sri Lanka, in 1983, and the M.A.Sc. and Ph.D. degrees (with near-perfect GPA) in electrical engineering from the University of Ottawa, Ottawa, ON, Canada, in 1987 and 1990, respectively.

He was the Director of the WiMed Research Centre and the Associate Dean–Higher Degree Research (HDR) of the Division of Information and Communication Sciences and directed the Centre for Collaboration in Electromagnetic and Antenna Engineering at Macquarie University. He has also served as a member of the Dean's Advisory Council and the Division Executive and the Head of the department several times. He is currently the Director of Innovations for Humanity Pty Ltd., Sydney, NSW, Australia. He is also the Distinguished Professor in electromagnetic and antenna engineering at the University of Technology Sydney, Sydney, and a Visiting Professor with Macquarie University, Sydney. Since 2002, his research team has been involved with research grants, contracts, and Ph.D. scholarships worth over 22 million dollars, including 15 Australian Research Council grants, without counting the 245 million-dollar SmartSat Corporative Research Centre, which started in 2019. He has provided expert assistance to more than a dozen companies, including Intel, Santa Clara, CA, USA; the Hewlett Packard Laboratory, Palo Alto, CA, USA; Cisco Systems, Sydney; Audacy, Santa Rosa, CA, USA; Cochlear, Sydney; Optus, Sydney; ResMed, Sydney; and Katherine-Werke, Munich, Germany. His team designed the high-gain antenna system for the world's first entirely Ka-band CubeSat made by Audacy and launched to space by SpaceX in December 2018. This is believed to be the first Australian-designed high-gain antenna system launched to space, since CSIRO-designed antennas in Australia's own FedSat launched in 2002. His research has been supported by many national and international organizations, including the Australian Research Council, Intel, the U.S. Air Force, Cisco Systems, Hewlett-Packard, the Australian Department of Defence, the Australian Department of Industry, the NSW Chief Scientist and Engineer Office, and German and Indian governments. He has authored over 650 research publications and his papers have been cited ∼12 500 times. In 2021, his publications received over 1400 citations. His H-index is 53 and i-10 is 212. In addition to the IEEE Kanda Award mentioned above, several of his papers have been among the most cited or most downloaded. For example, one he coauthored on All-metal Wideband Metasurface on *Scientific Reports* in May 2021 was selected by Web of Science-Clarivate as both a Highly Cited Paper (top 1% in the academic field of Engineering) as well as a Hot Paper (to 1% in Engineering). He is in world's top 100 000 most-cited scientists list by Mendeley Data.

Dr. Esselle is a fellow of the Royal Society of New South Wales and Engineers Australia. His most recent awards include the Top Space Award in Australia—the "Winner of Winners" Excellence Award—as well as the Academic of Year Award at the 2022 Australian Space Awards from the most prestigious Excellence Award, the Academic of the Year Award at 2021 Australian Defence Industry Awards, the Finalist for the 2021 Australian National Eureka Prize for Outstanding Mentor of Young Researchers, the Runner-up to the same prize in 2020, the 2019 Motohisa Kanda Award (from IEEE USA) for the most cited paper in IEEE TRANSACTIONS ON ELECTROMAGNETIC COMPATIBILITY in the past five years, the 2021 IEEE Region 10 (Asia-Pacific) Outstanding Volunteer Award, and the 2020 IEEE NSW Outstanding Volunteer Award. According to the special report on research published by The Australian national newspaper, he is the 2019 National Research Field Leader in Australia in both microelectronics and electromagnetism fields. Previously, he received the 2019 Macquarie University Research Excellence Award for Innovative Technologies, the 2019 ARC Discovery International Award, the 2017 Excellence in Research Award from the Faculty of Science and Engineering, the 2017 Engineering Excellence Award for Best Innovation, the 2017 Highly Commended Research Excellence Award from Macquarie University, the 2017 Certificate of Recognition from IEEE Region 10, the 2016 and 2012 Engineering Excellence Awards for Best Published Paper from the IESL NSW Chapter, the 2011 Outstanding Branch Counsellor Award from IEEE headquarters (USA), the 2009 Vice Chancellor's Award for Excellence in Higher Degree Research Supervision, and the 2004 Innovation Award for best invention disclosure. His mentees have been awarded many fellowships, awards, and prizes for their research achievements. Fifty-eight international experts who examined the theses of his Ph.D. graduates ranked them in the top 5% or 10%. Two of his students were awarded the Ph.D. degree with the highest honor at Macquarie University, the Vice Chancellor's Commendation, and one received University Medal for the Master of Research. From 2018 to 2020, he chaired the prestigious Distinguished Lecturer Program Committee of the IEEE Antennas and Propagation (AP) Society—the premier global learned society dedicated to antennas and propagation—which has close to 10 000 members worldwide. After two stages in the selection process, he was also selected by the IEEE Antennas and Propagation (AP) Society as one of two candidates in the ballot for the 2019 President of the Society. Only three people from Asia or Pacific apparently have received this honor in the 68-year history of this society. He is also one of the three distinguished lecturers (DLs) selected by this society in 2016. He is the only Australian to chair the AP DL Program ever, the only Australian AP DL in almost two decades, and the second Australian AP DL ever (after UTS Distinguished Visiting Professor Trevor Bird). He has served the IEEE AP Society Administrative Committee in several elected or *ex officio* positions from 2015 to 2020. He is also the Chair of the Board of management of Australian Antenna Measurement Facility. He was the elected Chair of IEEE New South Wales (NSW) in 2016 and IEEE NSW AP/MTT Chapter in 2017. He is in the College of Expert Reviewers of the European Science Foundation for the term 2019–22 and he has been invited to serve as an international expert/research grant assessor by several other research funding bodies as well, including the European Research Council and funding agencies in Norway, Belgium, The Netherlands, Canada, Finland, Hong Kong, Georgia, South Africa, and Chile. He has been invited by Vice-Chancellors of Australian and overseas universities to assess applications for promotion to professorial levels. He has also been invited to assess grant applications submitted to Australia's most prestigious schemes, such as Australian Federation Fellowships and Australian Laureate Fellowships. In addition to the large number of invited conference speeches he has given, he has been an invited plenary/extended/keynote/distinguished speaker of several IEEE and other venues over 30 times, including EuCAP 2020 Copenhagen, Denmark; URSI 2019, Seville, Spain; and 23rd ICECOM 2019, Dubrovnik, Croatia. He has served or is serving as a Senior Editor for IEEE ACCESS and an Associate Editor for IEEE TRANSACTIONS ON ANTENNAS PROPAGATION and *IEEE Antennas and Propagation Magazine*. He is the Track Chair of IEEE AP-S/URSI 2022 Denver, 2021 Singapore, and 2020 Montreal; the Technical Program Committee Co-Chair of ISAP 2015, APMC 2011, and TENCON 2013; and the Publicity Chair of ICEAA/IEEE APWC 2016, IWAT 2014, and APMC 2000. His research activities are posted on the web at http://web.science.mq.edu.au/∼esselle/ and https://www.uts.edu.au/staff/karu.esselle.

Dushmantha N. Thalakotuna (Senior Member, IEEE) received the B.Sc. degree in electronics and telecommunication from the University of Moratuwa, Moratuwa, Sri Lanka, in 2008, and the Ph.D. degree in electronic engineering from Macquarie University, Sydney, NSW, Australia, in 2012.

He is currently a Lecturer with the School of Electrical and Data Engineering, University of Technology Sydney, Sydney. From 2013 to 2019, he has worked in multiple radio frequency and systems engineering roles designing antennas and Monolithic Microwave Integrated Circuits (MMICs) and radio frequency (RF) systems for both commercial and defense industries. His current research interests include MMICs, SATCOM antennas, base station antennas, reconfigurable microwave and millimeter-wave circuits, metasurfaces, and periodic structures.

Dr. Thalakotuna serves as the Section Secretary for IEEE NSW and is a member of IEEE Antennas and Propagation Society and IEEE Microwave Theory and Techniques Society.